

Surface magnetism of hematite

G. S. Krinchik and V. E. Zubov

Moscow State University

(Submitted March 11, 1975)

Zh. Eksp. Teor. Fiz. **69**, 707-721 (August 1975)

The phenomenon of surface magnetism was investigated on natural faces of hematite. A theory of this phenomenon is constructed by calculating the energy of the surface anisotropy for faces of the type (100) and (111); it is shown that the surface-anisotropy energy has two values on each face, depending on the types of the Fe^{3+} ions situated in the surface layer; the behavior of the surface magnetic layer in an external field is calculated. The vanishing of the Morin point (T_M) in small hematite particles is explained. During the course of the experiments, effects of the erasure of the surface magnetism by a magnetic field were observed, but no complete destruction of the magnetism was obtained up to $H = 17$ kOe. It is concluded on the basis of the experimental data that the antiferromagnetism vector emerges from the basal plane on the surface of the basal and nonbasal faces of the hematite at $T > T_M$. Destruction of the surface magnetism was observed when the hematite single crystals were treated with acids.

PACS numbers: 73.20.-r, 75.30.Gw

1. INTRODUCTION

The influence of the surface on magnetic phenomena in crystals was investigated from a variety of points of view. Mention can be made, for example of effects of surface anisotropy in ferromagnets,^[1] the role of pinning of surface spins in the excitation of standing spin waves by a homogeneous magnetic field,^[2] the possibility of the onset of an uncompensated magnetic moment on the surface of a helicoidal antiferromagnet,^[3] the singular thermodynamic behavior of surface magnetism which follows from the theory of second-order phase transitions,^[4] the change of the band structure of a metal in the near-surface zone,^[5] the appearance of "dead" non-magnetic layers on the surface of a ferromagnet,^[6] the appearance of surface spin-wave modes in ferromagnets,^[7] the possible spin-wave contribution to the transition from ortho to para hydrogen on the surface of a magnet,^[8] the oscillatory dependence of the rate of the carbonylation of nickel on the magnetic field on the surface of Ni single crystals,^[9] and others.

In this article we consider one of the aspects of this general problem, namely the formation of a macroscopic magnetic transition layer as a result of the change in the symmetry of the surroundings of surface magnetic ions. This phenomenon was observed earlier^[10] by measuring the surface magnetic properties of nonbasal faces of hematite crystals by a magneto-optical method. Since the light at the employed wavelengths penetrated less than 0.1μ into the hematite, the magneto-optical method could be used to measure the magnetic characteristics of not the entire sample, but only of a thin surface layer. It turned out that the character of the magnetic state of the crystal in the volume and on the surface differ qualitatively. Thus, for example, although hematite is a crystal with an easy anisotropy plane, the surface magnetic layer is similar to an orthoferrite. Namely, the equatorial effect when the field is oriented along the line of intersection of the (111) and (100) plane is maximal and decreases to zero when the field is rotated to the direction [011] perpendicular to the indicated line in the (100) plane, although the magnetization component in this direction is $0.53m_s$ in the volume of the crystal. The component normal to the (100) plane is in this case $0.84m_s$, whereas experiment has shown the absence of a

polar effect up to a field $H = 8000$ Oe. The observed onset of a surface magnetic layer can be attributed to the lowering of the symmetry of the surroundings of the magnetic ions on the surface and to the appearance of additional terms in the expression for the energy of the magnetodipole interaction and the Dzyaloshinskiĭ interaction of the surface Fe^{3+} ions.

As shown by Artman and co-workers,^[11] the energy of the magnetic crystallographic anisotropy of hematite is due to two main types of interaction—energy of one-ion anisotropy and energy of the magnetodipole interaction of the magnetic Fe^{3+} ions. The contributions of these two types of interaction are opposite in sign and almost equal in magnitude, and therefore the resultant interaction at room temperature turns out to be smaller by two orders of magnitude than the main contributions. The condition that the interactions be approximately equal is violated near the surface of the crystal. It can be assumed, for simplicity, that the energy of the one-ion anisotropy of the magnetic Fe^{3+} ions, which is determined by the oxygen environment, changes little on the surface in comparison with the volume of the crystal. At the same time, the energy of the magnetodipole interaction of the surface ions should change significantly. The magnitude of this change is different for different types of crystal faces. Inasmuch as two large quantities of opposite sign become unbalanced on the surface, the anisotropy energy per surface Fe^{3+} ion should exceed the anisotropy energy per volume ion by two orders of magnitude. So large an additional surface anisotropy energy is sufficient to produce a macroscopic magnetic transition layer, in which the atomic magnetic moments are gradually rotated from one orientation to the other. The crystal is clothed by a unique magnetic "jacket" similar to a domain wall, but in this case the transition layer separates not two domains, but the crystal itself from its environment. The width of the produced magnetic layer can reach, according to the calculations, several microns. The produced surface layer is of fully macroscopic dimensions; its magnetic properties, which differ from the bulk properties, we shall call surface magnetism. The present article is devoted to an investigation of the surface magnetism produced on natural faces of hematite.

2. THEORY OF SURFACE MAGNETISM OF HEMATITE

A. The case $H = 0$.

The symmetry of the surface anisotropy energy σ_a , which is made up of the magnetodipole energies of the surface Fe^{3+} ions, is determined by the type of crystal face. For example, on the (111) face this energy should be isotropic with respect to rotation about the crystal axis, and on the (100) face σ_a should be invariant to reflection in a plane perpendicular to (100) and passing through [011] (Fig. 1). This is due to the fact that on the (100) face each Fe^{3+} ion is surrounded by other magnetic Fe^{3+} ions symmetrically relative to the indicated plane. The hematite surface anisotropy energy σ_a was calculated for faces of the type (100) and (111). The lattice of the magnetic Fe^{3+} ions of hematite can be represented as consisting of two primitive cubic sublattices imbedded one in the other in such a way that they form an almost-body-centered lattice. The unit cube is slightly elongated along one of the body diagonals (Fig. 2), and the Fe^{3+} ion, which is located inside the cube, is shifted along the same diagonal from the center by 8% of the length of the diagonal of this unit cube. The neighboring magnetic Fe^{3+} ions in each of the indicated sublattices have oppositely directed spins. It is important that the surface magnetodipole energy depends on the type of ion, 1 (3) or 2 (4), with which the face of the crystal terminates (see Figs. 2 and 3). This energy on the (100) face was calculated with allowance for the interaction of the Fe^{3+} ions in a cube with side $4a$ (Fig. 2) surrounding each given Fe^{3+} ion, and was calculated for the (111) face with allowance for the Fe^{3+} ions situated in a cylinder of radius $2.7a$ and height $5.3a$. The magnetodipole energy converges rapidly with increasing number of ions included in the calculation, owing to the high symmetry of the lattice of the Fe^{3+} ions, and also because the neighboring magnetic ions in the elementary cubic sublattices of these ions have opposite spin directions. We present below expressions for the energy densities of the surface anisotropy (in erg/cm^2) in the indicated approximation:

$$\sigma_{a(100)}^1 = -0.1 \sin^2 \theta \cos^2 \varphi + 0.1 \sin^2 \theta \sin^2 \varphi - 0.01 \cos^2 \theta - 0.25 \sin \theta \cos \theta \sin \varphi,$$

$$\sigma_{a(100)}^2 = 0.24 \sin^2 \theta \cos^2 \varphi - 0.03 \sin^2 \theta \sin^2 \varphi - 0.21 \cos^2 \theta + 0.04 \sin \theta \cos \theta \sin \varphi,$$

$$\sigma_{a(111)}^1 = 0.24 \cos^2 \theta, \quad \sigma_{a(111)}^2 = -0.24 \cos^2 \theta. \quad (1)$$

For comparison we present the energy densities with allowance for the interaction with the nearest neighbors:

$$\sigma_{a(100)}^1 = -0.14 \sin^2 \theta \cos^2 \varphi + 0.13 \sin^2 \theta \sin^2 \varphi + 0.02 \cos^2 \theta - 0.18 \sin \theta \cos \theta \sin \varphi,$$

$$\sigma_{a(100)}^2 = 0.26 \sin^2 \theta \cos^2 \varphi + 0.02 \sin^2 \theta \sin^2 \varphi - 0.24 \cos^2 \theta + 0.18 \sin \theta \cos \theta \sin \varphi,$$

$$\sigma_{a(111)}^1 = 0.04 \cos^2 \theta, \quad \sigma_{a(111)}^2 = -0.2 \cos^2 \theta,$$

θ and φ are the spherical angles of the vector L (Fig. 1). As a control, we calculated also the magnetodipole energy of the crystal hematite in the volume. It turned out to equal $0.89 \times 10^7 \cos^2 \theta \text{ erg/cm}^3$. The corresponding value obtained in [11] is equal to $0.92 \times 10^7 \cos^2 \theta \text{ erg/cm}^3$.

The equilibrium angles θ_0 and φ_0 of the vector L on the surface face, in the absence of an external magnetic field, are determined by the competition of the surface anisotropy energy and the energy of the transition magnetic layer, which is characterized, if anisotropy in the basal plane is neglected, by the change of the angle θ ,

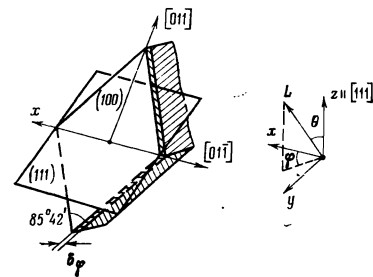


FIG. 1. Schematic representation of the nonbasal face (100) of hematite and intersection with the basal (111) plane; the employed rectangular coordinate system is shown on the right.

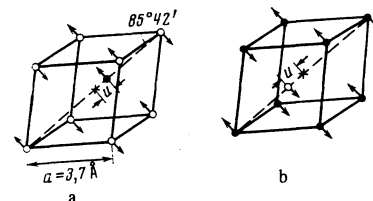


FIG. 2. Distorted elementary cube of the Fe^{3+} ions of hematite. u —displacement of the Fe^{3+} ion from the center of the cube. Figures 2a and 2b show two cases of the termination of the (100) faces, with different types of the Fe^{3+} ions in the surface layer. The lattice parameters were taken or calculated from the data of [12].

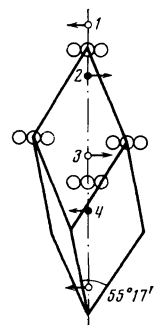


FIG. 3. Schematic representation of the unit cell of hematite in the rhombohedral setting.

from the equilibrium value θ_0 on the surface to the equilibrium value in the volume. The thermodynamic potential of hematite [13], with allowance for the terms that are principal in this case and are determined by the inhomogeneity of the distribution of the vector L and by the crystallographic anisotropy energy, is given by the expression

$$\Phi = \frac{A_1}{2} \left[\left(\frac{\partial l_\alpha}{\partial x} \right)^2 + \left(\frac{\partial l_\alpha}{\partial y} \right)^2 \right] + \frac{A_2}{2} \left(\frac{\partial l_\alpha}{\partial z} \right)^2 + \frac{a}{2} l_z^2, \quad (2)$$

where $\alpha = x, y, z$; A_1 and A_2 are the exchange parameters; a is the uniaxial anisotropy constant; $l = (\mathbf{I}_1 - \mathbf{I}_2)/2I_0$ is the reduced antiferromagnetism vector ($|\mathbf{I}_1| = |\mathbf{I}_2| = I_0$ are the magnetizations of the hematite sublattices in the two-sublattice model). For an arbitrary crystal face, expression (2) can be represented in the form

$$\Phi = \frac{A}{2} \left(\frac{d\theta}{ds} \right)^2 + \frac{a}{2} \cos^2 \theta, \quad (3)$$

where the parameter A is expressed in terms of A_1 and A_2 and the angle of inclination of the face to the z axis; s is the distance from the start of the face into the interior of the crystal. Then the energy of the surface transition layer per unit face area is

$$\gamma_\theta = \frac{1}{2} \int_0^{\theta_0} \left\{ A \left(\frac{d\theta}{ds} \right)^2 + a \cos^2 \theta \right\} ds. \quad (4)$$

Depending on the temperature, the hematite can be in different magnetic states, namely at $0^\circ\text{K} < T < T_M < 260^\circ\text{K}$ the spins of the magnetic Fe^{3+} ions are directed along the crystal axis ($a < 0$), and at $T_M < T < T_N \approx 950^\circ\text{K}$ the spins are perpendicular to this axis ($a > 0$). The boundary conditions of the problem of calculating the transition layer take in these two cases the forms

$$\theta|_{s=0} = \theta_0, \quad \theta|_{s=\infty} = 0 \quad \text{at } 0 < T < T_M, \quad (5)$$

$$\theta|_{s=0} = \theta_0, \quad \theta|_{s=\infty} = \pi/2 \quad \text{at } T_M < T < T_N, \quad (6)$$

where θ_0 is arbitrary. The form of the function $\theta(s)$, which minimizes the energy γ_θ (4) is determined by the solution of the corresponding Euler equation. For the case (5) we have

$$\cos \theta = \text{th} \left(\frac{s+s_0}{\delta_0} \right) = \frac{\cos \theta_0 + \text{th}(s/\delta_0)}{1 + \cos \theta_0 \text{th}(s/\delta_0)}, \quad (7)$$

$$\gamma_\theta = \gamma_{\theta_0} (1 - \cos \theta_0),$$

where

$$s_0 = -\delta_0 \ln \text{th} \frac{\theta_0}{2}, \quad \delta_0 = \left(\frac{A}{|a|} \right)^{1/2}, \quad \gamma_{\theta_0} = (|a|A)^{1/2}.$$

For the case (6) we have

$$\sin \theta = \text{th} \left(\frac{s+s_0}{\delta_0} \right) = \frac{\sin \theta_0 + \text{th}(s/\delta_0)}{1 + \sin \theta_0 \text{th}(s/\delta_0)}, \quad (8)$$

$$\gamma_\theta = \gamma_{\theta_0} (1 - \sin \theta_0),$$

where

$$s_0 = \delta_0 \ln \text{th} \left(\frac{\pi}{4} + \frac{\theta_0}{2} \right), \quad \delta_0 = \left(\frac{A}{a} \right)^{1/2}, \quad \gamma_{\theta_0} = (aA)^{1/2}.$$

Let us find the effective thickness δ of the transition layer, which we define in terms of the derivative $ds/d\theta$ at $\theta = \theta_0$ and the interval of variation of the angle θ , which is equal, say for the case (8), to $(\pi/2 - \theta_0)$. We then have

$$\delta_0 = \left. \frac{ds}{d\theta} \right|_{\theta=\theta_0} \left(\frac{\pi}{2} - \theta_0 \right) = \frac{\pi/2 - \theta_0}{\cos \theta_0} \delta_{00}. \quad (9)$$

For the two limiting cases $\theta_0 \ll 1$ and $\pi/2 - \theta_0 \ll 1$ we obtain approximately the following expressions:

$$1) \delta_0 \approx (1/2\pi - \theta_0) \delta_{00} \quad \text{at } \theta_0 \ll 1, \quad (9a)$$

$$2) \delta_0 \approx [1 + 1/6(1/2\pi - \theta_0)^2] \delta_{00} \quad \text{at } 1/2\pi - \theta_0 \ll 1. \quad (9b)$$

Let us estimate δ_{00} and γ_{θ_0} . For hematite, the exchange constant is $B \approx 10^4$ cgs emu, and the anisotropy constant is $a \approx 4 \times 10^5$ erg/cm³; [14] $A \sim B I_0^2 c^2$, where $I_0 \approx 920$ G is the magnetization of each of the sublattices, calculated with allowance for the fact that each Fe^{3+} ion has a magnetic moment $5\mu_B$ (μ_B is the Bohr magneton), $c \approx 1.9 \text{ \AA}$ is the distance between the layers of the Fe^{3+} ions. Then $A \approx 0.3 \times 10^{-5}$ erg/cm and

$$\delta_{00} \approx 2.7 \cdot 10^{-4} \text{ cm}, \quad \gamma_{\theta_0} \approx 1.1 \text{ erg/cm}^2. \quad (10)$$

We have neglected in (10) the possible anisotropy of the parameter A . The presented estimates of the width and of the energy of the transition layer are valid for temperatures that are far enough from the temperature T_M at which a vanishes.

To determine the equilibrium magnetic structure

near the crystal face it is necessary to find the minimum of the sum of the energy of the surface anisotropy σ_a and the energy of the transition layer γ_θ as a function of the variables θ_0 and φ_0 . Since we have neglected the contribution made to the thermodynamic potential (2) by the anisotropic terms in the basal plane it follows that φ_0 is determined by the minimum of $\sigma_a = \sigma_a(\varphi_0)$. The table lists the equilibrium values of θ_0 and φ_0 for the faces (100) and (111) and two types of face termination, obtained by solving the equations $\partial(\sigma_a + \gamma_\theta)/\partial\theta_0 = 0$ and $\partial\sigma_a/\partial\varphi_0 = 0$.

For σ_a we used expression (1), and for γ_θ expressions (7) and (8). It is seen from the table that generally speaking a weak ferromagnetic moment should exist on the (100) faces below the Morin point (T_M) for both types of face termination; in the case of termination 1, the theoretically predicted magnetic moment on the surface is of the order of 30% of the magnetic moment at $T_M < T < T_N$. At $T > T_M$, for a termination of the face (100) of type 1, the magnetization on this face, in the absence of a magnetic field, is directed along the y axis (see Fig. 1), and in the case of termination of type 2 the magnetization is parallel to the x axis, and in this case there is no normal component of \mathbf{m}_s on the (100) face. On the face (111), the magnetodipole surface energy is insufficient to change the magnetic symmetry of the surface layer in comparison with the volume. However, the surface anisotropy can play a significant role in thin hematite plates, comparable in thickness with the transition layer (9), i.e., $\sim 300 \text{ \AA}$. Then for samples with type of termination 1 there will be no Morin point on the (111) face, and at $0 < T < T_N$ these samples will be in a weak ferromagnetic state, while the samples with type of termination 2 will be antiferromagnetic in this temperature interval. Yamamoto [15] has shown that in small hematite particles the Morin point decreases with decreasing particle dimensions. In particular, he has shown that starting with a certain critical dimension of the particles, which amounted from 200 to 600 \AA for various groups of samples, the Morin temperature drops practically to 0°K . The critical dimension of the particles in his paper is in good agreement with our estimate ($\sim 300 \text{ \AA}$).

In bulky samples, the surface anisotropy can lead to a shift of the Morin point in the surface layer, owing to the decrease of γ_{θ_0} in (7) and (8). Indeed, in the region of the Morin point the uniaxial anisotropy constant depends approximately linearly on T [11]:

$$a(T) \approx a'(T_M)(T - T_M), \quad (11)$$

where $a'(T_M) = (\partial a / \partial T)_{T=T_M} \approx 0.06 \cdot 10^5$ erg/cm³deg. [14]

If we substitute (11) in formulas (7) and (8) for γ_{θ_0} and then determine the equilibrium value of θ_0 on the surface of the (111) face, then we find that the Morin point shifts by $\sim 10^\circ\text{K}$.

It should be noted, however, that experimental observation of the surface magnetic layer at $T < T_M$ on bulky samples of hematite is difficult if the usual switching magneto-optical procedure is used, based on reversing the magnetization of the sample. This is due to the fact that the surface magnetic layer cannot reverse the magnetization of the entire volume of the sample (or rotate all the spins in the volume through 180°) if the sample is in the antiferromagnetic state.

Equilibrium values of the spherical angles θ_0 and φ_0 of the vector \mathbf{L} on the surfaces of the faces (100) and (111) of hematite crystals above and below the Morin point, calculated by minimizing the sum of the surface-anisotropy energy σ_a and the energy of the magnetic transition layer in the absence of a magnetic field, for two types of face termination

Temperature	Crystal face	Type of termination	φ_0	θ_0
$T < 250$ K	(100)	1	$1/2\pi$ ($9/2\pi$)	0.19 ($\pi - 0.19$)
		2	$3/2\pi$ ($1/2\pi$)	0.03 ($\pi - 0.03$)
	(111)	1	—	0
		2	—	0
$250 \text{ K} < T < 950$ K	(100)	1	0 (π)	$1/2\pi$
		2	$3/2\pi$ ($1/2\pi$)	$1/2\pi - 0.04$ ($1/2\pi + 0.04$)
	(111)	1	—	$1/2\pi$
		2	—	$1/2\pi$

B. The case $H \neq 0$.

We consider the behavior of a surface magnetic layer in an external field in the case of greatest interest to us that of the (100) face at $T_M < T < T_N$. We shall not take into account the deviation of the angle θ from $\pi/2$, since it has been shown that the value of $(\pi/2 - \theta_0)$ on the (100) face is small (see the table). We shall henceforth also show that the φ -width of the transition layer is much smaller than the θ -width of the transition layer in a magnetic field up to values such that the φ transition layer vanishes completely. The thermodynamic potential of the crystal in the magnetic field, which depends on the angle φ , can be expressed as follows:

$$\Phi = \frac{H_D H_t}{B} \sin(\psi - \varphi) + \frac{H_t^2}{2B} \cos^2(\psi - \varphi), \quad (12)$$

where H_t is the projection of the field on the basal plane of the crystal, and ψ is the angle between \mathbf{H}_t and the x axis (Fig. 1). The first term in (12) determines the energy of the spontaneous magnetic moment \mathbf{m}_s , [16] and the second determines the energy of the moment induced in an external magnetic field. We do not take into account in (12) the contribution from the exchange invariant of fourth order $(1/2)D(\mathbf{l} \cdot \mathbf{m})^2$. [16] As seen from the structure of this invariant, its order of magnitude is given by the expression $(1/2)D(\mathbf{l} \cdot \mathbf{m})^2 \sim (1/2)D(\chi_{\parallel} H_{\parallel})^2$, where $D \cong 3.3 \times 10^5$ cgs emu, $\chi_{\parallel} \sim 5.0 \times 10^{-6}$ cgs emu is the longitudinal antiferromagnetic susceptibility, [14] and $H_{\parallel} \sim 10^4$ Oe is the external-field component parallel to \mathbf{l} . Then $(1/2)D(\mathbf{l} \cdot \mathbf{m})^2 \sim 0.5 \times 10^3$ erg/cm³, whereas $H_D H_t / B \sim H_t^2 / 2B \sim 10^4$ erg/cm³. Actually the magnitude of the fourth-order exchange term will be smaller, since \mathbf{l} is rotated perpendicular to \mathbf{H}_t in the surface layer in a field ~ 20 kOe (see Fig. 4), and therefore H_{\parallel} does not reach the value 10^4 Oe. Thus, neglect of the indicated terms is justified.

Taking into account the inhomogeneity of the magnetic structure, we rewrite (12) in analogy with (3):

$$\Phi = \frac{A}{2} \left(\frac{d\varphi}{ds} \right)^2 + \frac{H_D H_t}{B} \sin(\psi - \varphi) + \frac{H_t^2}{2B} \cos^2(\psi - \varphi) \quad (13)$$

The function $\varphi(H_t, s)$ is determined by solving the Euler equation for the integral

$$\gamma_0 = \int_0^{\infty} \left\{ \frac{A}{2} \left(\frac{d\varphi}{ds} \right)^2 + \frac{H_D H_t}{B} \sin(\psi - \varphi) + \frac{H_t^2}{2B} \cos^2(\psi - \varphi) \right\} ds. \quad (14)$$

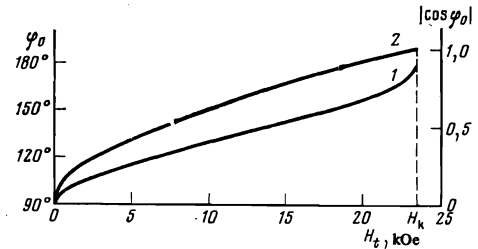


FIG. 4. Dependence of the equilibrium value of $\varphi_0(H_t)$ at $H_t \parallel y$ on the surface of the (100) face with termination of type 2 (curve 1), and plot of the projection of the magnetic moment $\cos \varphi_0(H_t)$ on the y axis (curve 2).

The Euler equation takes the form

$$\frac{d\varphi}{ds} = \pm \frac{1}{\delta_{\varphi_0}} \sin x (1 - k^2 \sin^2 x)^{1/2}, \quad (15)$$

where

$$k^2 = \frac{\beta}{\alpha + \beta}, \quad \delta_{\varphi_0} = \frac{1}{(\alpha + \beta)^{1/2}}, \quad \alpha = \frac{4H_D H_t}{AB}, \quad \beta = \frac{4H_t^2}{AB}, \quad x = \frac{\pi}{4} + \frac{\psi}{2} - \frac{\varphi}{2},$$

The boundary conditions of the problem are

$$x|_{s=0} = x_0 = \frac{\pi}{4} + \frac{\psi}{2} - \frac{\varphi_0}{2}, \quad x|_{s=\infty} = \frac{\pi}{4} + \frac{\psi}{2} - \frac{\psi + \pi/2}{2} = 0. \quad (16)$$

The solution of (15) with allowance for the boundary conditions is

$$s/\delta_{\varphi_0} = \ln \left| \frac{\Delta + \cos x}{\Delta - \cos x} \right|_x^x, \quad (17)$$

where $\Delta = (1 - k^2 \sin^2 x)^{1/2}$.

Expression (17) can be represented in the form

$$\sin(\psi - \varphi) = \left[1 - (2 - k^2) \text{th}^2 \left(\frac{s + s_{\varphi_0}}{2\delta_{\varphi_0}} \right) \right] / \left[1 - k^2 \text{th}^2 \left(\frac{s + s_{\varphi_0}}{2\delta_{\varphi_0}} \right) \right],$$

where

$$s_{\varphi_0} = \delta_{\varphi_0} \ln \frac{\Delta(x_0) + \cos x_0}{\Delta(x_0) - \cos x_0}.$$

Later on, for the determination of φ_0 on the surface, we shall need an expression for $\partial \gamma_0 / \partial \varphi_0$. To this end, we rewrite (14) with allowance for (15):

$$\gamma_0 = \frac{A}{\delta_{\varphi_0}^2} \int_0^{\infty} \sin^2 x (1 - k^2 \sin^2 x) ds, \quad ds = \frac{\delta_{\varphi_0} d\varphi}{\sin x (1 - k^2 \sin^2 x)^{1/2}}.$$

Then

$$\frac{\partial \gamma_0}{\partial \varphi_0} = \frac{\partial}{\partial \varphi_0} \left\{ \frac{A}{\delta_{\varphi_0}^2} \int_0^{\infty} \sin^2 x (1 - k^2 \sin^2 x) ds \right\} = \frac{\partial}{\partial \varphi_0} \left\{ \frac{A}{\delta_{\varphi_0}} \int_{x_0}^{\infty} \sin x (1 - k^2 \sin^2 x)^{1/2} d\varphi \right\}, \quad (18)$$

$$\frac{\partial \gamma_0}{\partial \varphi_0} = -\frac{A}{\delta_{\varphi_0}} \sin x_0 (1 - k^2 \sin^2 x_0)^{1/2} = -\gamma_{\varphi_0} \sin x_0 (1 - k^2 \sin^2 x_0)^{1/2}.$$

Let us estimate δ_{φ_0} and γ_{φ_0} . For hematite $H_D \cong 2.2 \times 10^4$ Oe, $B \cong 10^4$ cgs emu, [14] and $A \cong 0.3 \times 10^{-5}$ erg/cm. Hence

$$\delta_{\varphi_0} \cong \frac{0.59 \cdot 10^{-3}}{[H_t(1 + H_t/H_D)]^{1/2}} \text{ [cm]}, \quad \gamma_{\varphi_0} \cong 0.51 \cdot 10^{-2} \left[H_t \left(1 + \frac{H_t}{H_D} \right) \right]^{1/2} \left[\frac{\text{erg}}{\text{cm}^2} \right] \quad (19)$$

The surface-anisotropy energy of the (100) face at $\theta = \pi/2$ (see the table) is of the form (see (1))

$$\sigma_{a(100)}^{1,2} = b \cos^2 \varphi_0 + d \sin^2 \varphi_0 = b + (d-b) \sin^2 \varphi_0, \quad (20)$$

φ_0 is then determined from the condition that the sum of the energies γ_φ and $\sigma_{a(100)}^{1,2}$ be a minimum:

$$\frac{\partial}{\partial \varphi_0} (\gamma_\varphi + \sigma_{a(100)}^{1,2}) = -\gamma_{\varphi_0} \sin x_0 (1 - k^2 \sin^2 x_0)^{1/2} + (d-b) 2 \sin \varphi_0 \cos \varphi_0 = 0. \quad (21)$$

Let us consider a particular case: the face (100) has a termination of type 2, and $\psi = \pi/2$ (\mathbf{H}_t is parallel to the y axis). Then (21) takes the form

$$-\gamma_{\varphi_0} \cos \frac{\varphi_0}{2} \left(1 - k^2 \cos^2 \frac{\varphi_0}{2}\right)^{1/2} + (d-b) \sin 2\varphi_0 = 0. \quad (22)$$

Equation (22) determines the function $\varphi_0(\mathbf{H}_t)$ which is plotted on Fig. 4 for $d-b \cong -0.27$ (type 2 termination of the face (100)) and γ_{φ_0} from (19). The same figure shows a plot of $\cos \varphi_0(\mathbf{H}_t)$, which determines the projection of the magnetization on the surface of the face on the field \mathbf{H}_t at $\psi = \pi/2$.

We determine also the effective width δ_φ of the transition layer for this case. In analogy with (9) we have

$$\delta_\varphi = \frac{ds}{d\varphi} \Big|_{\varphi=\varphi_0} (\pi - \varphi_0) = \frac{\delta_{\varphi_0} (\pi - \varphi_0)}{\cos^{1/2} \varphi_0 (1 - k^2 \cos^2 \varphi_0)^{1/2}}, \quad (23)$$

where $\pi/2 \leq \varphi_0 \leq \pi$. We introduce for convenience $\varphi'_0 = \varphi_0 - \pi/2$. We then obtain for the two limiting cases from (23):

- 1) $H_t \ll H_k$ (see Fig. 4), $\varphi'_0 \ll 1$, $\delta_\varphi \cong (2.2 - 0.3\varphi'_0) \delta_{\varphi_0}$;
- 2) $H_t \ll H_k$, $\pi/2 - \varphi'_0 \ll 1$, $\delta_\varphi \cong 2\delta_{\varphi_0}$.

Consequently, the effective width is $\delta_\varphi \approx 2\delta_{\varphi_0}$. For $H_t = 1000$ Oe we have $\delta_\varphi \cong 0.4 \mu$ and $\gamma_{\varphi_0} \cong 0.16$ erg/cm².

3. EXPERIMENTAL INVESTIGATION OF SURFACE MAGNETISM

Measurements of the Kerr effect were carried out at room temperature on natural basal and nonbasal faces of synthetic single crystals of hematite, as functions of the external magnetic field. The employed samples had faces of area 5–10 mm², and the type of the face was determined by x-ray diffraction. The magneto-optical setup consisted of a DMR-4 monochromator, an incandescent lamp light source, a U2-6 measuring tuned amplifier, and a V9-2 synchronous detector capable of raising the signal/noise ratio and of determining the phase of the investigated signal. The sample magnetization was reversed with magnets capable of producing an alternating magnetic field of amplitude up to 13.5 kOe in measurements of the equatorial Kerr effect and up to 17 kOe in measurements of the polar Kerr effect. The indicated values of the alternating magnetic field were obtained by using closed iron cores for the electromagnets and by using a TU-600 high-power amplifier. The closed magnet core made it possible to decrease considerably the level of the magnetic static induced in the photoreceiver and to measure reliably magneto-optical effects of magnitude $\sim 5 \times 10^{-6}$. An FEU-79 photomultiplier was used to register the light reflected from the sample.

Figure 5 shows the field dependences of the polar Kerr effect in the nonbasal face (100) of a hematite single crystal. Curves 1 and 2 were obtained in a field normal to the (100) face, curve 1a was obtained in a field parallel to the [011] axis, and curve 1b in a field parallel to the [01 $\bar{1}$] axis (Fig. 1). The absence of a polar Kerr effect

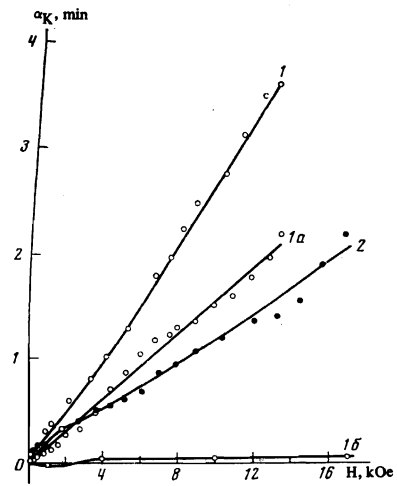


FIG. 5. Plots $\alpha_K(H)$ of the polar Kerr effect on the nonbasal face (100) of single-crystal hematite ($\lambda = 0.55\mu$). Curves 1 and 2 were plotted in a field $\mathbf{H} \perp (100)$, curve 1a in a field $\mathbf{H} \parallel [011]$, curve 1b in a field $\mathbf{H} \parallel [01\bar{1}]$. The axes were set with accuracy $\sim 3^\circ$. Curve 2 was plotted several months after curves 1, 1a and 1b for the same sample.

in weak fields allows us to conclude that in the investigated sample the growth of the (100) face terminated with Fe^{3+} ions of type 2 (see Sec. 2 and Figs. 2 and 3). The appearance of the polar Kerr effect in these measurements can be naturally attributed to gradual "erasure" of the surface magnetism: to rotation of the vector \mathbf{L} in the surface layer, to the decrease of the width of the layer under the influence of the external magnetic field, and to the consequent appearance of a normal component of the magnetization on the (100) face (see Sec. 2). The difference between the values of the effect for curves 1, 1a, and 1b is due to the difference between the values of the components of the erasing field \mathbf{H}_t , namely H_t is approximately equal to 0.84H, 0.53H, and zero for the direction normal to (100), the [011] direction, and the [01 $\bar{1}$] direction, respectively. As seen from Fig. 5, the surface magnetism has not vanished completely in a field $H = 13.5$ kOe (curve 1) or 17 kOe (curve 2). According to the calculations (Sec. 2), for the case when the field is perpendicular to the (100) face, complete rotation of the vector \mathbf{L} , which is perpendicular to the field H_t , should take place at $H = H_k/0.84 \approx 28$ kOe, which does not contradict the experimental data. Figure 6 shows the dependence of the polar Kerr effect on the direction of the magnetic field in the (100) plane at $H = 4$ kOe. The change in the magnitude and sign of the fact are explained in natural fashion as being due to the change in the magnitude and sign of the projection of the external field on the y axis (Fig. 1) when the sample is rotated.

Figure 7 shows typical plots of the equatorial Kerr effect against the field for the directions [01 $\bar{1}$] (curves 1, 2, 3) and [011] (curves 1a, 2a, 3a)). The onset and the growth of the effect on curves 1a, 3a, and 3a can be explained in analogy with the appearance and growth of the polar Kerr effect with the field on Fig. 5, but in this case the magnitude of the effect is determined by the magnetization component along the [011] axis. It can also be analogously concluded that the growth of the faces of the investigated crystals has terminated with Fe^{3+} ions of type 2. Thus, we have qualitative agreement between the measurements of the polar (Fig. 5) and the quatorial Kerr effects (Fig. 7). Namely, the appearance and growth of a normal component of the spontaneous magnetization on the (100) face, which manifest themselves in a growth

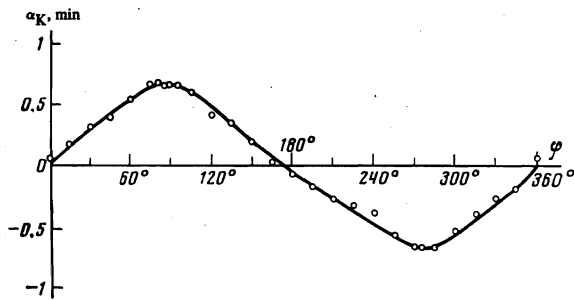


FIG. 6. Polar Kerr effect α_K on the (100) face vs. the field direction in the (100) plane ($\lambda = 0.55\mu$). At $\varphi = 0$ we have $H \parallel [011]$ ($H = 4$ kOe).

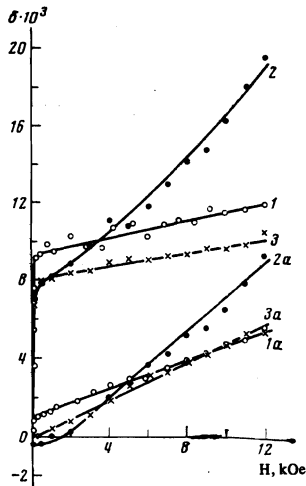


FIG. 7. Equatorial Kerr effect $\delta(H)$ in a field $H \parallel [01\bar{1}]$ (curves 1, 2, 3) and in a field $H \parallel [011]$ (curves 1a, 2a, 3a) ($\lambda = 0.53\mu$). Curves 2 and 2a were plotted half a year after curves 1 and 1a for the same sample. Curves 3 and 3a were obtained with a different sample on which the work was performed for a short time. The light-incidence angle was 70° .

of the polar effect, are accompanied by a growth of the spontaneous magnetization in the $[011]$ direction, which is confirmed by the field dependence of the equatorial Kerr effect at $H \parallel [011]$. This relation between the components of the spontaneous magnetic moment in the direction normal to (100) and the direction $[011]$ is connected with the fact that in hematite the vector m_s can lie only in the (111) plane^[16], and it was shown in^[17] that the magneto-optical effects in $\alpha\text{-Fe}_2\text{O}_3$ are determined precisely by the presence of a normal component of the spontaneous magnetization in the case of the polar Kerr effect and the projection of m_s on the external field in the case of the equatorial Kerr effect.

Comparison of the $\cos \theta_0(H_t)$ curve on Fig. 4, which describes the rotation of the vector L on the surface of the (100) face under the influence of an external field parallel to the y axis, with the curves of the polar (Fig. 5) and equatorial (Fig. 7) Kerr effects, shows that on the whole the calculated curve accounts for the dependence of the measured effects on the field. There is a difference, however, between the indicated curves at low values of the field, namely, $\cos \varphi_0 \sim (H_t)^{1/2}$, while $\alpha_K \sim H_t$ and $\delta \sim H_t$. This difference may be connected with the presence, on the surface of the face, of interactions that are small in comparison with magnetodipole energy and depend linearly on the small deviation of the angle φ from the equilibrium value $\varphi_0(H = 0)$. Such a contribution can be made, for example, by the Dzyaloshinskii energy^[10] or by the one-ion anisotropy of the Fe^{3+} surface ions (see Sec. 4).

4. POSSIBILITY OF EMERGENCE OF THE ANTI-FERROMAGNETISM VECTOR FROM THE BASAL PLANE IN THE SURFACE LAYER

In measurements of the equatorial Kerr effect on nonbasal faces of hematite in a field $H \parallel [011]$ (Fig. 7, curves 1, 2, 4), and also on the basal faces in a field $H \parallel (111)$ (Fig. 8), it was observed that the magnitude of the effect and the slopes of the $\delta(H)$ curves are different on different samples. It was also noted that in the case of prolonged work with one and the same sample, the magnitude of the effect on this sample decreases in both the easy $[01\bar{1}]$ and the difficult $[011]$ directions. The curves shown in Fig. 9 were plotted several weeks after curves 1 and 1a on Fig. 7 for one and the same sample. The effect was particularly strongly altered in the difficult direction. It is as if the magnetization were in this case in a strongly "frozen" state. An impression is gained that the "working" of the sample surface by the magnetic field or by the light during the measurement stabilizes the state of the surface ions and causes a corresponding "freezing" of the surface magnetism. It is possible that this "working" of the surface is analogous to the process that occurs in directed ordering in the course of heat treatment in a magnetic field. It is interesting that after a "recovery" lasting about one or two months the sample "unfreezes" (curves 2 and 2a in Fig. 2). Curve 2 of Fig. 5 was obtained at the same time as curves 2 and 2a of Fig. 7, with the same sample. Thus, even though the sample "unfroze," it went over into a state different from the initial one (cf. curves 1 and 2 on Fig. 5 and curves 1 and 2 or 1a and 2a on Fig. 7). The possibility of the described "freezing" of the magnetization on the surface of the sample can explain why no erasure of the surface magnetism on the non-basal faces of hematite single crystals were observed in^[10] at all.

It is clear that the changes of the magnitude and field dependences of the magneto-optical properties on the surface of the crystal are due to changes of the magnetic state of the Fe^{3+} ions in the surface layer or in layers close to it. This may be due to the influence of the energy of the one-ion anisotropy of the surface Fe^{3+} ions, which should depend strongly on the character of the surrounding of these ions by the oxygen anions O^{2-} (the so-called reconstruction of the crystal surface^[18]). In

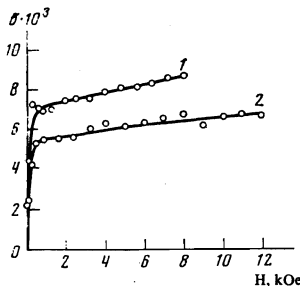


FIG. 8

FIG. 8. Equatorial Kerr effect on the basal face (111) of $\alpha\text{-Fe}_2\text{O}_3$ ($\lambda = 0.54\mu$). Curves 1 and 2 were plotted with the same sample with a time difference of about half a year.

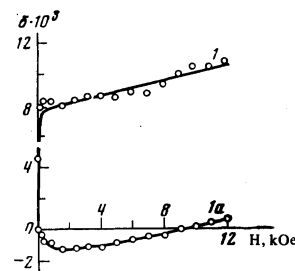


FIG. 9

FIG. 9. Equatorial Kerr effect in the easy $[01\bar{1}]$ (curve 1) and difficult $[011]$ (curve 1a) directions, measured after prolonged work (about two months) with the sample used to plot curves 1 and 1a in Fig. 7 ($\lambda = 0.53\mu$).

Sec. 1 we have assumed the one-ion anisotropy to be the same on the surface as in the volume. In particular, the surface one-ion anisotropy can cause the equilibrium value of θ_0 on the surface of the (100) face to differ significantly from $\pi/2$ at $T > T_M$, and this in turn can lead to a decrease of the surface-layer magnetization. From the form of curves 1a and 2a on Fig. 7 and curve 1a on Fig. 9 at small H it can be assumed that the energy of the one-ion anisotropy of the surface Fe^{3+} ions sometimes takes the equilibrium position of the antiferromagnetism vector \mathbf{L} on the surface out of the symmetry plane of the hematite crystal ($\varphi_0 \neq \pi/2$, Fig. 1) in the absence of an external field, which leads to the presence of magnetization in the surface layer, and consequently to the presence of an equatorial Kerr effect in the difficult direction [011] at small H.

If θ_0 on the surface of the sample face differs from $\pi/2$, then in an external field the spin system in the surface layer will rotate in such a way that $\pi/2 - \theta_0$ tends to zero. It is necessary here to distinguish between two mechanisms that lead to the indicated rotation. The first mechanism is analogous to the rotation of the spins perpendicular to the field and is realized in the presence of a field component perpendicular to the basal plane (111). The field of the jumplike spin rotation in the volume of the hematite amounts to 50–60 kOe.^[14] The second mechanism is realized in a field parallel to (111), and is due to the change of the Dzyaloshinskiĭ energy in this field.^[19] The spins rotate in a plane perpendicular to H so that their projection on (111) increases. A complete rotation of the spins from $\theta = 0$ to $\theta = \pi/2$ is effected in hematite, for example at $T \cong 200^\circ\text{K}$ in a field $H \sim 80$ kOe.^[14] As seen from these figures, the explanation offered above for the observed change of the effect in the easy direction [011] with increasing field is reasonable. Similar arguments apply also to the basal faces of the hematite (Fig. 8). Namely, owing to the one-ion anisotropy of the surface ions, the vector \mathbf{L} on the surface of the (111) face emerges from the basal plane; the magnitude of the effect is determined by the extent to which θ_0 differs from $\pi/2$, and in an external field θ_0 approaches $\pi/2$, in which case the effect increases. The emergence of \mathbf{L} from (111) is easiest to produce if the (111) face has a termination of type 2 (see (1)).

One more circumstance, which may be of importance in the interpretation of magneto-optical measurements, must be borne in mind. As seen from Fig. 7 (curve 2a), Fig. 9 (curve 1a), and Fig. 10 (curve 1), the equatorial Kerr effect on the surface of the (100) face can have a negative sign, and also a negative slope of the $\delta(H)$ curve) (see Fig. 10, curve 1). It is possible that this phenomenon is due to the interaction of the light with the inhomogeneous magnetic structure of the transition

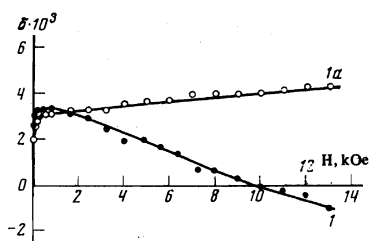


FIG. 10. Plots of the equatorial Kerr effect in a field $\mathbf{H} \parallel [01\bar{1}]$ (curve 1) and in a field $\mathbf{H} \parallel [011]$ (curve 1a), obtained with the same sample as curve 1a in Fig. 11 ($\lambda = 0.53\mu$).

layer. But since the parameters of the magnetic transition layer change in an external magnetic field, this can lead to an additional dependence of the effect δ on the field H.

5. CHANGE OF THE CHARACTER OF THE SURFACE MAGNETISM

As shown in Sec. 2, the character of the surface magnetism of hematite depends on the type of Fe^{3+} ions (1 or 2) making up the last plane of the crystal face (see Figs. 2 and 3 and the table). If the (100) face terminates in Fe^{3+} ions of type 1, then the easy-magnetization direction is the y axis (Fig. 1). On the other hand if the last magnetic layer terminates in Fe^{3+} ions of type 2, then the easy-magnetization axis coincides with the x axis, as was indeed observed in all the investigated samples. This raises the natural question: is it possible to change in some way the character of the surface magnetism, or at least produce a state intermediate between the two indicated above? One of these methods may be etching the nonbasal faces of the $\alpha\text{-Fe}_2\text{O}_3$ with acids that dissolve hematite. Figure 11 shows plots of the polar effect $\alpha_K(H)$ in a field $\mathbf{H} \parallel [011]$ before (curves 1 and 2) and after (curves 1a and 2a) etching the samples in acids. The sample for which curve 1a is plotted was kept in 30% sulfuric acid for 30 hours. Curve 2a was obtained with a sample etched with 30% hydrochloric acid for 16 hours. As seen from Fig. 11, after etching, a polar effect appeared in the samples in a weak field, i.e., an effect that is connected with the magnetization of the sample to saturation, and not with the destruction of the surface magnetism in the magnetic field.

Figure 10 shows plots of the equatorial Kerr effect $\delta(H)$ for the same sample as used to plot curve 1a of Fig. 11, in the easy [011] and difficult [011] directions. As expected an equatorial Kerr effect from the component $m_S^y \parallel y$ appears on the sample together with the polar effect, and can be interpreted as a consequence of the chemical destruction of the surface magnetism (in the case of curve 2a on Fig. 11 one must apparently speak of partial destruction).

The decrease of the effect $\delta(H)$ in Fig. 10 in a field $\mathbf{H} \parallel [01\bar{1}]$, and also the reversal of its sign, seem to be connected with the change discussed at the end of the preceding section, in the conditions of light reflection from the face of the sample with increasing field. The difference between the values of the polar effect for different samples (curves 1a and 2a of Fig. 11), and also

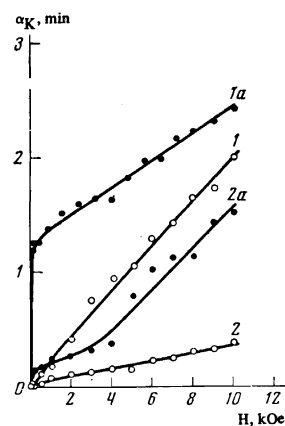


FIG. 11. Plots of the polar effect $\alpha_K(H)$ obtained in a field $\mathbf{H} \parallel [011]$ before (curves 1 and 2) and after (curves 1a and 2a) etching the $\alpha\text{-Fe}_2\text{O}_3$ samples with nonbasal (100) faces ($\lambda = 0.55\mu$). The first sample (curves 1 and 1a) was etched in 30% sulfuric acid for 30 hours, and the second sample (2 and 2a) in 30% hydrochloric acid for 16 hours.

the relatively small value of the equatorial Kerr effect on Fig. 10, can be attributed to the emergence of the vector L from the basal plane in the transition layer (see Sec. 4).

The sample etched in sulfuric acid was investigated also with a magneto-optic setup having a resolution on the order of microns.^[20] The area of the investigated section of the sample surface was $\sim 10 \mu^3$. As shown by the measurements, magnetization saturation was reached in a field ~ 10 Oe. The entire surface of the sample, with area $\sim 6 \text{ mm}^2$, turned out to be homogeneous, i.e., the polar and equatorial Kerr effect were practically identical over the entire surface. We can conclude therefore that if the macroscopic sections with different types of Fe^{3+} ions in the surface layer (and consequently with a different character of the surface magnetism) do exist, then their area is less than $10 \mu^2$.

It should be noted that among the hematite samples etched with acids, with faces of the (100) type, there were some with higher chemical stability, on which the character of the surface magnetism was not altered even by prolonged treatment with acid (for several days).

¹L. Neel, *J. Phys. Radium* **15**, 225 (1954).

²C. Kittel, *Phys. Rev.* **110**, 1295 (1958); M. H. Seavy and P. E. Tannenwald, *Phys. Rev. Lett.* **1**, 168 (1958).

³L. N. Bulaevskii and V. L. Ginzburg, *Fiz. Metal. Metalloved.* **17**, 631 (1964).

⁴M. I. Kaganov and A. N. Omel'yanchuk, *Zh. Eksp. Teor. Fiz.* **61**, 1679 (1971) [*Sov. Phys.-JETP* **34**, 895 (1972)]; M. I. Kaganov, *Zh. Eksp. Teor. Fiz.* **62**, 1196 (1972) [*Sov. Phys.-JETP* **35**, 631 (1972)].

⁵R. Haydock, Volker Heine, M. J. Kelly, and J. B. Pendry, *Phys. Rev. Lett.* **29**, 868 (1972).

⁶L. Liberman and J. Clinton, *AIP Conf. Proc.* **10**, part 2, Magnetism and Magnetic Materials, 1972, 18th

Annual Conference, Denver, ed. C. D. Graham, Jr. and J. J. Phyne, p. 1531; J. C. Walker, C. R. Guarnieri, and R. Semper, p. 1539.

⁷R. E. De Wames and T. Wolfram, *Phys. Rev.* **185**, 720 (1969).

⁸E. Ilisca, *Phys. Rev. Lett.* **24**, 797 (1970).

⁹G. S. Krinchik and R. A. Shvartsman, *Zh. Eksp. Teor. Fiz.* **67**, 2326 (1974) [*Sov. Phys.-JETP* **40**, 1153 (1975)].

¹⁰G. S. Krinchik, A. P. Khrebtov, A. A. Askochenskiĭ, and V. E. Zubov, *Pis'ma Zh. Eksp. Teor. Fiz.* **17**, 466 (1973) [*JETP Lett.* **17**, 335 (1973)].

¹¹J. O. Artman, J. C. Murphy, and S. Foner, *Phys. Rev.* **138**, A912 (1965).

¹²Yu. A. Izyumov and R. P. Ozerov, *Magnitnaya neŭtronografiya* [*Magnetic Neutron Diffraction Practice*], Nauka, 1966.

¹³M. M. Farztdinov, *Izv. AN SSSR ser. fiz.* **28**, 580 (1964).

¹⁴R. A. Voskanyan, R. Z. Levitin, and V. A. Shurov, *Zh. Eksp. Teor. Fiz.* **53**, 459 (1967) [*Sov. Phys.-JETP* **26**, 302 (1968)]; *ibid.* **54**, 790 (1968) [**27**, 423 (1968)]; R. Z. Levitin and V. A. Shurov, *Pis'ma Zh. Eksp. Teor. Fiz.* **7**, 142 (1968) [*JETP Lett.* **7**, 110 (1968)].

¹⁵N. Yamamoto, *J. Phys. Soc. Japan* **24**, 23 (1968).

¹⁶I. E. Dzyaloshinskiĭ, *Zh. Eksp. Teor. Fiz.* **32**, 1547 (1957) [*Sov. Phys.-JETP* **5**, 1259 (1957)].

¹⁷G. S. Krinchik and V. E. Zubov, *Pis'ma Zh. Eksp. Teor. Fiz.* **20**, 307 (1974) [*JETP Lett.* **20**, 137 (1974)].

¹⁸G. A. Somorjai and H. H. Farrell, *Adv. Chem. Phys.* **20**, 215 (1971).

¹⁹G. Cinader and S. Shtrikman, *Solid State Commun.* **4**, 459 (1966); V. I. Ozhogin and V. G. Shapiro, *Pis'ma Zh. Eksp. Teor. Fiz.* **6**, 467 (1967) [*JETP Lett.* **6**, 7 (1967)].

²⁰G. S. Krinchik and O. M. Benidze, *Zh. Eksp. Teor. Fiz.* **67**, 2180 (1974) [*Sov. Phys.-JETP* **40**, 1081 (1975)].

Translated by J. G. Adashko

76